



HAL
open science

Glutathionyl-hydroquinone reductases from poplar are plastidial proteins that deglutathionylate both reduced and oxidized glutathionylated quinones

Pierre-Alexandre Lallement, Edgar Meux, José M. Gualberto, Stéphane Dumarcay, Frédérique Favier, Claude Didierjean, Frederick Saul, Ahmed Haouz, Mélanie Rouhier, Éric Gelhaye, et al.

► To cite this version:

Pierre-Alexandre Lallement, Edgar Meux, José M. Gualberto, Stéphane Dumarcay, Frédérique Favier, et al.. Glutathionyl-hydroquinone reductases from poplar are plastidial proteins that deglutathionylate both reduced and oxidized glutathionylated quinones. *FEBS Letters*, 2015, 589 (1), pp.37 - 44. 10.1016/j.febslet.2014.11.021 . hal-01522015

HAL Id: hal-01522015

<https://hal.univ-lorraine.fr/hal-01522015>

Submitted on 12 May 2017

HAL is a multi-disciplinary open access archive for the deposit and dissemination of scientific research documents, whether they are published or not. The documents may come from teaching and research institutions in France or abroad, or from public or private research centers.

L'archive ouverte pluridisciplinaire **HAL**, est destinée au dépôt et à la diffusion de documents scientifiques de niveau recherche, publiés ou non, émanant des établissements d'enseignement et de recherche français ou étrangers, des laboratoires publics ou privés.



Glutathionyl-hydroquinone reductases from poplar are plastidial proteins that deglutathionylate both reduced and oxidized glutathionylated quinones



Pierre-Alexandre Lallement^{a,b}, Edgar Meux^{a,b}, José M. Gualberto^c, Stéphane Dumarçay^d, Frédérique Favier^{e,f}, Claude Didierjean^{e,f}, Frederick Saul^g, Ahmed Haouz^g, Mélanie Morel-Rouhier^{a,b}, Eric Gelhaye^{a,b}, Nicolas Rouhier^{a,b}, Arnaud Hecker^{a,b,*}

^a Université de Lorraine, Interactions Arbres – Microorganismes, UMR1136, F-54500 Vandœuvre-lès-Nancy, France

^b INRA, Interactions Arbres – Microorganismes, UMR1136, F-54280 Champenoux, France

^c Institut de Biologie Moléculaire des Plantes, CNRS-UPR 2357, 67084 Strasbourg, France

^d Laboratoire d'Etudes et de Recherches sur le Matériau Bois, EA 1093, Vandœuvre-lès-Nancy F-54506, France

^e Université de Lorraine, CRM², Equipe BioMod, UMR 7036, Faculté des Sciences et Technologies, BP 70239, 54506 Vandœuvre-lès-Nancy, France

^f CNRS, CRM², Equipe BioMod, UMR 7036, Faculté des Sciences et Technologies, BP 70239, 54506 Vandœuvre-lès-Nancy, France

^g Institut Pasteur, Plate-Forme de Cristallographie, CNRS-UMR3528, 75724 Paris, France

ARTICLE INFO

Article history:

Received 22 July 2014

Revised 4 November 2014

Accepted 15 November 2014

Available online 29 November 2014

Edited by Stuart Ferguson

Keywords:

Deglutathionylation
Glutathione transferase
Plastid
Poplar

ABSTRACT

Glutathionyl-hydroquinone reductases (GHRs) catalyze the deglutathionylation of quinones via a catalytic cysteine. The two GHR genes in the *Populus trichocarpa* genome, *Pt-GHR1* and *Pt-GHR2*, are primarily expressed in reproductive organs. Both proteins are localized in plastids. More specifically, *Pt-GHR2* localizes in nucleoids. At the structural level, *Pt-GHR1* adopts a typical GHR fold, with a dimerization interface comparable to that of the bacterial and fungal GHR counterparts. *Pt-GHR1* catalyzes the deglutathionylation of both reduced and oxidized glutathionylated quinones, but the enzyme is more catalytically efficient with the reduced forms.

© 2014 Federation of European Biochemical Societies. Published by Elsevier B.V. All rights reserved.

1. Introduction

Recent plant genome analyses identified at least 14 classes of glutathione transferases (GSTs), namely Tau, Phi, Zeta, Theta, Lambda, EF1B γ , Metaxin, Ure2p, Hemerythrin, Iota, TetraChloro-HydroQuinone Dehalogenase (TCHQD), dehydroascorbate reductase (DHAR), microsomal ProstaGlandin E-Synthase type 2 (mPGES-2) and glutathionyl-hydroquinone reductases (GHRs) [1–4]. These GHRs, which are found in bacteria, haloarchaea, fungi and plants, constitute a newly defined GST class due to their ability to reduce glutathionyl-quinones, but not glutathionyl-acetophenone derivatives unlike the closely related Omega GSTs (GSTOs/GTOs) [5–9]. In bacteria, GHRs participate to the reductive dehalogenase pathway as shown for *Sphingobium chlorophenolicum* PcpF whereas the role of *Escherichia coli* YqjG is not clearly established

[6,10]. In *Saccharomyces cerevisiae*, the three GHRs were initially referred to as GTO1, GTO2/ECM4 and GTO3 and GTO1 was shown to be involved in sulfur metabolism [11]. In plants, the physiological substrates and functions of GHRs are unknown.

GHRs exhibit a quite conserved CPWA active site sequence, thus belonging to the cysteine-containing GSTs (Cys-GSTs), which also include GSTOs, Lambda and Beta GSTs (GSTLs and GSTBs) and DHARs [12–14]. The presence of the catalytic cysteine is required for deglutathionylation activities [6,8,9,15] as for other Cys-GSTs and glutaredoxins (Grxs) [16,17]. Unlike canonical GSTs, GHRs adopt a particular dimeric quaternary arrangement, defining a new GST structural class named Xi [8,18]. In these proteins, the two monomers associate exclusively via their α -helical domains. Another difference is the presence of a sequence insertion between $\alpha 2$ and $\beta 2$ and of a unique C-terminal extension. Moreover, the active site contains a conserved tyrosine triad which provides an acid/base catalytic assistance in the reaction mechanism [18].

We report the first characterization of the plant GHR family by studying the transcript level and subcellular localization of the two

* Corresponding author at: Université de Lorraine, Interactions Arbres – Microorganismes, UMR1136, F-54500 Vandœuvre-lès-Nancy, France.

E-mail address: arnaud.hecker@univ-lorraine.fr (A. Hecker).

Populus trichocarpa representatives (Pt-GHR1 and Pt-GHR2), and analyzing the enzymatic and structural properties of Pt-GHR1.

2. Materials and methods

2.1. RT-PCR experiments

RNA extraction from eight *P. trichocarpa* tissues and cDNA synthesis were performed as described by Lallement et al. [16]. Transcripts of Pt-GHR1 (Potri.015G121600), Pt-GHR2 (Potri.014G192300) and ubiquitin (Potri.015G013600), used as the reference gene, were amplified by PCR (25, 30 or 35 cycles) using specific primer pairs (Table S1).

2.2. Subcellular localization of GFP fusion proteins

Pt-GHR1 and Pt-GHR2 coding sequences, with or without the sequences coding for transit peptides, were amplified by PCR from petiole cDNAs with the primers shown in Table S1 and cloned in the pCK-GFP3 vector, upstream and in frame with the GFP coding sequence [19]. The PEND::dsRED construct was used as a control to localize plastidial nucleoids [20]. Young leaves of *Nicotiana benthamiana* were transfected by bombardment as described before [16]. After 18 h, fluorescence of GFP and chlorophyll were observed in leaves respectively at 505–550 nm and beyond 575 nm after excitation at 488 nm on a Zeiss LSM510 confocal microscope. The dsRED fluorescence was excited at 555 nm and observed at 560–615 nm.

2.3. Cloning in bacterial expression vectors and site-directed mutagenesis

Sequences coding for Pt-GHR1 and Pt-GHR2 devoid of the targeting sequences were inserted into pET-28a vector using primers shown in Table S1. For Pt-GHR1, the expressed protein is devoid of the first 34 amino acids. For Pt-GHR2, three constructs deprived of the 54, 57 and 86 N-terminal amino acids were tested. The catalytic cysteine of Pt-GHR1 was substituted by a serine (C49S) or an alanine (C49A) from pET-28a::Pt-GHR1 using mutagenic oligonucleotides (Table S1) and the QuikChange site-directed mutagenesis kit (Agilent Technologies).

2.4. Protein expression and purification

The *E. coli* Rosetta2 (DE3) pLysS strain transformed with pET-28a::Pt-GHR1 wild-type and mutants was grown at 37 °C in LB medium containing kanamycin (50 µg ml⁻¹) and chloramphenicol (34 µg ml⁻¹). At OD_{600nm} of 0.7, 0.5% (v/v) of ethanol was added to the medium and cells were cooled to 4 °C for 3 h. Protein expression was subsequently induced for 16 h at 20 °C with 0.1 mM isopropyl β-D-1-thiogalactopyranoside. Cells were harvested and resuspended in a 30 mM Tris-HCl pH 8.0, 200 mM NaCl buffer. After lysis by sonication, the cell extract was centrifuged (35000×g, 25 min, 4 °C). After differential fractionation with ammonium sulfate (40% and 80% saturation), recombinant proteins were purified by size exclusion chromatography (Ultrogel[®] ACA44, Biosepra) and then by ion exchange chromatography (DEAE-cellulose column, Sigma). The purified proteins were stored in 30 mM Tris-HCl pH 8.0, 200 mM NaCl buffer at –20 °C and concentrations were determined using theoretical molar absorption coefficients of 55997.5 M⁻¹ cm⁻¹ for Pt-GHR1 and 55935 M⁻¹ cm⁻¹ for Pt-GHR1 C49S and C49A variants. *Phanerochaete chrysosporium* GHR1 (Pc-GHR1) and *E. coli* YqjG (Ec-YqjG) were obtained as described previously [8].

2.5. Determination of the oligomerization states and molecular masses

Native or reduced GHRs were analyzed either by mass spectrometry as described previously [8] or by size exclusion chromatography onto a calibrated Superdex 200 10/300 column (GE Healthcare). Reduced proteins were obtained by incubation for 1 h with a 10 fold excess of dithiothreitol (DTT) at room temperature.

2.6. Crystallization and structure determination of recombinant Pt-GHR1

Details of crystallization, data collection and structure determination of Pt-GHR1 are described in [Supplementary Materials and Methods](#). Atomic coordinates and structure factors have been deposited in the Protein Data Bank under the accession code 4USS.

2.7. Substrate preparation

Glutathionylated phenylacetophenone (PAP-SG), menadione (MEN-SG), tetralone (TETRA-SG) and quercetin (Q-SG) were prepared as previously described [16,21–23] and analyzed by mass spectrometry. To generate menadiol-SG, 3 mM NaBH₄ were added to menadione-SG immediately before enzymatic analyses to avoid rapid re-oxidation into menadione-SG. The substrates (menadione-SG and menadiol-SG) and enzymatic products (menadione and menadiol) were analyzed by LC-MS. Liquid chromatography was performed at 40 °C on a Luna C18 100A column (2 mm × 150 mm, 3 µm, Phenomenex) with a 20 series Shimadzu Prominence UPLC system. The elution was performed with a methanol gradient in water containing 0.1% formic acid. Mass spectrometry detection was carried out with a Shimadzu TQD LC-MS8030 simultaneously in positive and negative ion mode after electrospray ionization.

2.8. Enzymatic activities

Thiol-transferase and DHAR activities were tested using hydroxyethyl disulfide (HED) and dehydroascorbate (DHA) respectively, peroxidase activity using H₂O₂, ter-butyl-hydroperoxide or cumene hydroperoxide, deglutathionylation activity using PAP-SG, TETRA-SG and Q-SG, esterase activity using 5-chloromethyl-fluorescein diacetate (Green CMFDA[®], Invitrogen) and glutathionylation activity using 1-chloro-2,4-dinitrobenzene (CDNB), phenethyl-isothiocyanate (phenethyl ITC) and p-nitrophenyl butyrate (PnP butyrate). All these procedures have been described previously [16].

Deglutathionylation of menadione-SG/menadiol-SG was assayed in 30 mM Tris-HCl pH 8.0, 1 mM EDTA buffer by following the appearance of deglutathionylated products by UV/visible spectrophotometry with or without a separation by HPLC. For the assay relying uniquely on spectrophotometric measurements, the enzyme and substrate concentrations of the reaction mixture are provided in the figure legends. For the assay involving the HPLC separation of the substrate and the product, the reaction was initiated by adding enzymes, and stopped after 20 s by adding a final concentration of 35% (v/v) ethanol and vigorous mixing. After centrifugation (14000×g for 15 min), the reaction products were analyzed by HPLC using a calibrated Gemini 5 µ C18 110A column (3 mm × 150 mm, Phenomenex) equilibrated with water containing 30 mM acetic acid pH 4.16 and 10% acetonitrile at 20 °C by monitoring absorbance at 250 nm. The nature of reaction products was confirmed by LC-MS (see above).

Deglutathionylation of GSH-conjugated 1,4-benzoquinone (BQ-SG) and 2-chloro-1,4-benzoquinone (ClBQ-SG) was measured by UV/visible spectrophotometric assays at 25 °C in a 30 mM Tris-HCl pH 8.0, 1 mM EDTA buffer. Molar extinction coefficients of BQ-SG and ClBQ-SG (respectively $\epsilon_{309\text{nm}} = 2451 \text{ M}^{-1} \text{ cm}^{-1}$ and $\epsilon_{318\text{nm}} = 3124 \text{ M}^{-1} \text{ cm}^{-1}$) were determined after complete reaction of known quinone concentrations with GSH [24]. The wavelengths were selected for maximal differences in the absorption spectra of GSH-conjugated vs non-conjugated quinones. To determine kinetic parameters, the decrease in absorbance was monitored after adding enzymes (0.2–1 μM depending on the substrates) to varying concentrations of BQ and ClBQ (5–280 μM) with 4 mM GSH.

For all activity assays, three independent experiments were performed at each substrate concentration. K_m and k_{cat} values were calculated with a Michaelis–Menten non-linear regression model using GraphPad Prism 5 software.

3. Results and discussion

3.1. Analysis of gene expression and subcellular localization of poplar GHRs

Two GHR genes, *Pt-GHR1* and *Pt-GHR2*, were identified in the *P. trichocarpa* genome. The corresponding proteins exhibit the characteristic CPWA signature and an N-terminal sequence which is predicted to be a chloroplastic targeting signal. The major difference compared to GSTLs and GSTOs is the presence of an insertion of about 40 residues in the N-terminal domain and a final C-terminal extension of 50–60 residues. According to the presence of an N-terminal targeting sequence, the transient expression of GHR::GFP fusions in tobacco leaves revealed chloroplastic localizations for both proteins (Fig. 1A and C). Control experiments performed with sequences devoid of the transit peptide resulted in cytosolic localization (Fig. 1B and E). For *Pt-GHR2*, depending on the cells and on

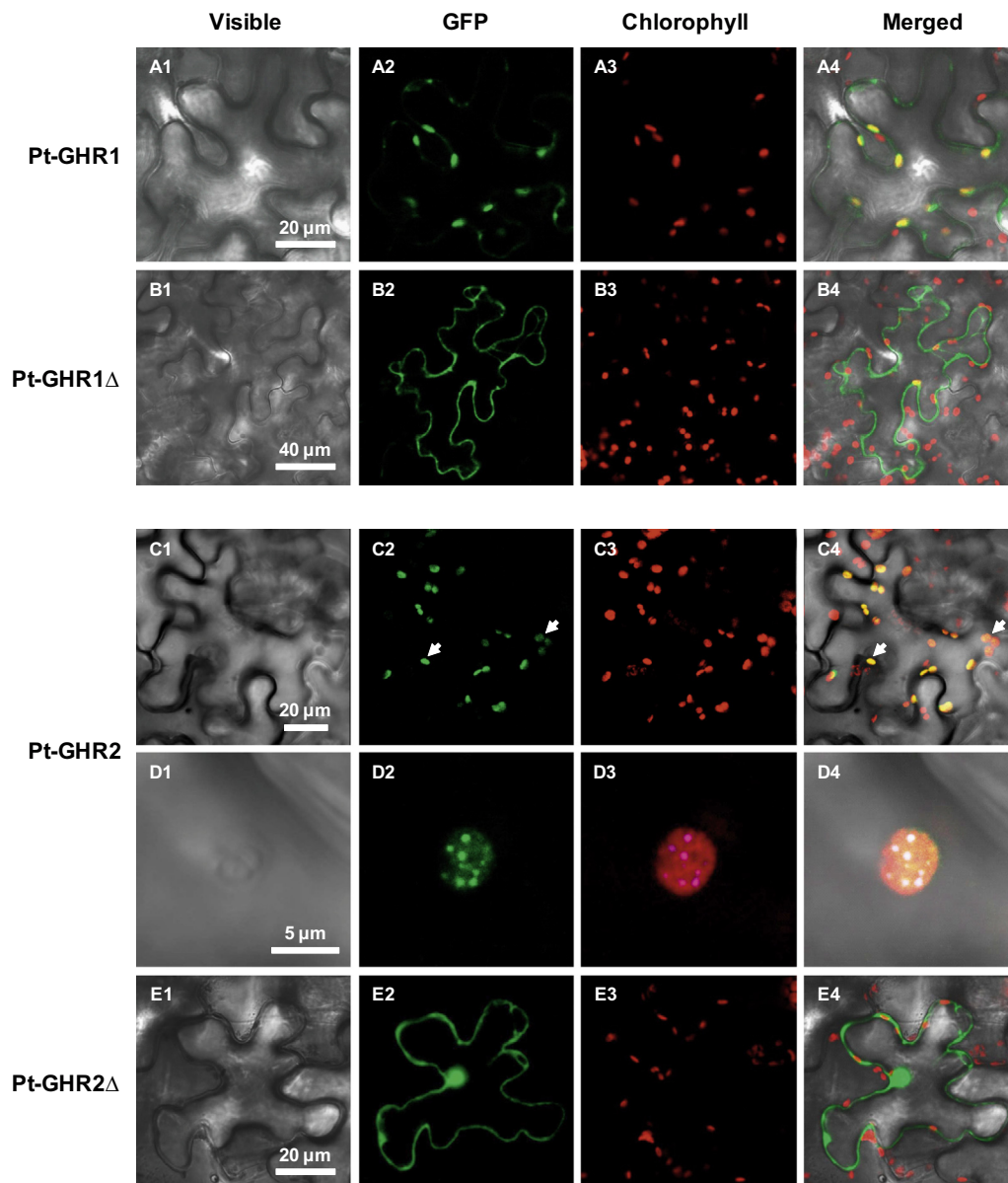


Fig. 1. Subcellular localization of Pt-GHRs. GFP fusions of *Pt-GHR1* (A, B) and *Pt-GHR2* (C, D and E) with (A, C and D) or without (B and E) targeting sequences were expressed in *Nicotiana benthamiana* young leaves. From left to right: (1) visible light; (2) fluorescence of the construct (green); (3) autofluorescence of chlorophyll (red); (4) merged images. In D3, autofluorescence of chlorophyll (red) is superimposed to fluorescence (magenta) of At-PEND fused to DsRed showing plastidial nucleoids. For *Pt-GHR2*, white arrows in C2 and C4 panels highlight the two types of fluorescence signals in chloroplasts.

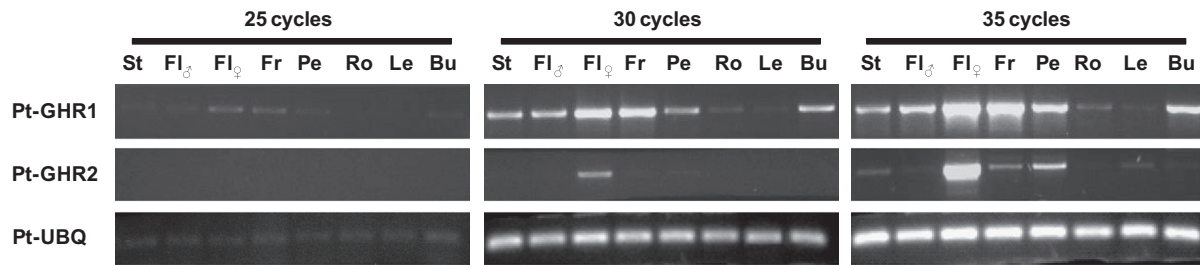


Fig. 2. Expression of Pt-GHR genes in selected poplar organs. Transcript levels were analyzed by RT-PCR after 25, 30 or 35 PCR cycles in stamens (St), male (FI_♂) and female (FI_♀) flowers, fruits (Fr), petioles (Pe), roots (Ro), leaves (Le) and buds (Bu). Ubiquitin was used as a housekeeping reference gene.

chloroplasts, the fluorescence signal was observed in stroma (Fig. 1C) and also in punctate structures corresponding to nucleoids (Fig. 1C and D) as confirmed by using the PEND::DsRED nucleoid marker [20,25]. This dual targeting raises questions concerning in particular the physiological function and the nature of the substrates associated to each sub-localization. In order to investigate the tissular gene expression pattern of *Pt-GHR1* and *Pt-GHR2*, RT-PCR experiments were performed from eight different tissues of a naturally growing *P. trichocarpa* tree (Fig. 2). *Pt-GHR1* transcripts were detected in all tissues tested but were more abundant in female flowers and fruits. Although *Pt-GHR2* transcripts were primarily found in female flowers, they could also be detected in stamens, fruits, petioles and leaves after 35 PCR cycles. Considering the observed chloroplastic localization of GHRs in tobacco leaves, it is surprising that the transcripts are present primarily in reproductive organs but are almost absent in leaves of the adult tree. These expression patterns indicate that they may have a more general plastidial localization and that they could have specialized functions related to the metabolism of these specific organs.

3.2. Poplar recombinant GHR1 is a dimeric enzyme isolated in a glutathionylated form

For biochemical and structural investigations, the mature forms of Pt-GHR1 and Pt-GHR2 were expressed in *E. coli* as recombinant proteins. After purification, 30 mg of soluble protein per liter of culture were obtained for Pt-GHR1. Although we have expressed three versions of Pt-GHR2 with different N-terminal targeting peptide cleavage sites, and either untagged or tagged with C-terminal hexahistidine- or strep-tags (the strep-tagII used consists of the WSHPQFEK sequence), none of these yielded satisfying amounts of soluble protein. They were either totally insoluble when using a procedure similar to the one used for GHR1 or formed soluble aggregates devoid of enzymatic activity when using an increased NaCl concentration. Thus, only Pt-GHR1 and variants whose catalytic cysteine residue was replaced by a serine (C49S) or an alanine (C49A) were characterized. Using analytical size exclusion chromatography, both Pt-GHR1 and Pt-GHR1 C49S were eluted as a single peak corresponding to an apparent molecular weight of about 78kDa (Table S2), compatible with a dimeric organization in solution similar to other reported GHRs [8,18]. Mass spectrometry analyses showed that Pt-GHR1 was present as two separated species, one with a molecular weight corresponding to a protein in which the N-terminal methionine is cleaved and another one with an additional mass increment of 305Da (Table S2). On the contrary, Pt-GHR1 C49S and reduced Pt-GHR1 are present as single species with cleaved methionines. These results indicated that a glutathione moiety is covalently bound to the catalytic cysteine, as already observed in other Cys-GSTs and Grxs [8,12,13,16,17,21]. Accordingly, a single species with a 305Da increment was observed after treating reduced Pt-GHR1 with disulfide glutathione (GSSG).

3.3. Structural analysis of poplar GHR1

The crystal structure of Pt-GHR1 in complex with glutathione was determined to a resolution of 2.5 Å (Table 1). Pt-GHR1 crystallized in the space group $P2_12_12$ with one monomer in the asymmetric unit. Continuous electron density was seen from residues 18 to 323. The dimer is generated by a crystallographic twofold axis (Fig. 3A). Initial Fourier difference maps revealed significant electron density attributed to glutathione in the G-site (Fig. 3B). The distance of 3.2 Å between the sulfur atoms of glutathione and of Cys49 did not fall within the range of expected disulfide bond length (~2.05 Å). Since GSH was covalently bound to recombinant Pt-GHR1, the intermolecular disulfide bridge was most likely cleaved during the X-ray data collection.

Table 1
Statistics of X-ray diffraction data collection and model refinement.

	Pt-GHR1
Data collection	
Beam line	PX1, SOLEIL
Space group	$P2_12_12$
Nb of monomers in the ASU ^a	1
Cell dimensions <i>a</i> , <i>b</i> , <i>c</i> (Å)	36.53, 92.41, 86.90
Resolution (Å)	19.66–2.50 (2.64–2.50) ^b
<i>R</i> _{merge}	0.16 (0.79)
Mean <i>I</i> / σ (<i>I</i>)	12.1 (3.0)
Completeness (%)	99.6 (82.1)
<i>n</i> Observations	115,601 (16,767)
Redundancy	10.8 (10.9)
Wilson B factor (Å ²)	36
Phasing method^c	
MR	
Refinement	
Resolution (Å)	19.50–2.50 (2.75–2.50)
<i>n</i> Reflections	10702 (2479)
Cutoff	$F > 0\sigma$ (<i>F</i>)
<i>R</i> _{all} (%) ^d	18.6
<i>R</i> _{free} (%) ^d	23.3 (31.1)
Average B-factor (Å²)	
Protein atoms	40
Ligand atoms	48
Solvent atoms	34
Ramachandran statistics (%)	
Preferred regions	97.4
Allowed regions	2.6
Outlier residues	0.0
R.m.s.^e deviations	
Bond length (Å)	0.003
Bond angle (°)	0.67

^a ASU: asymmetric unit.

^b Values in parentheses are for highest resolution shell.

^c MR: molecular replacement.

^d *R*_{all} was determined from all the reflections (working set + test set), whereas *R*_{free} corresponds to a subset of reflections (test set).

^e R.m.s.: root mean square.

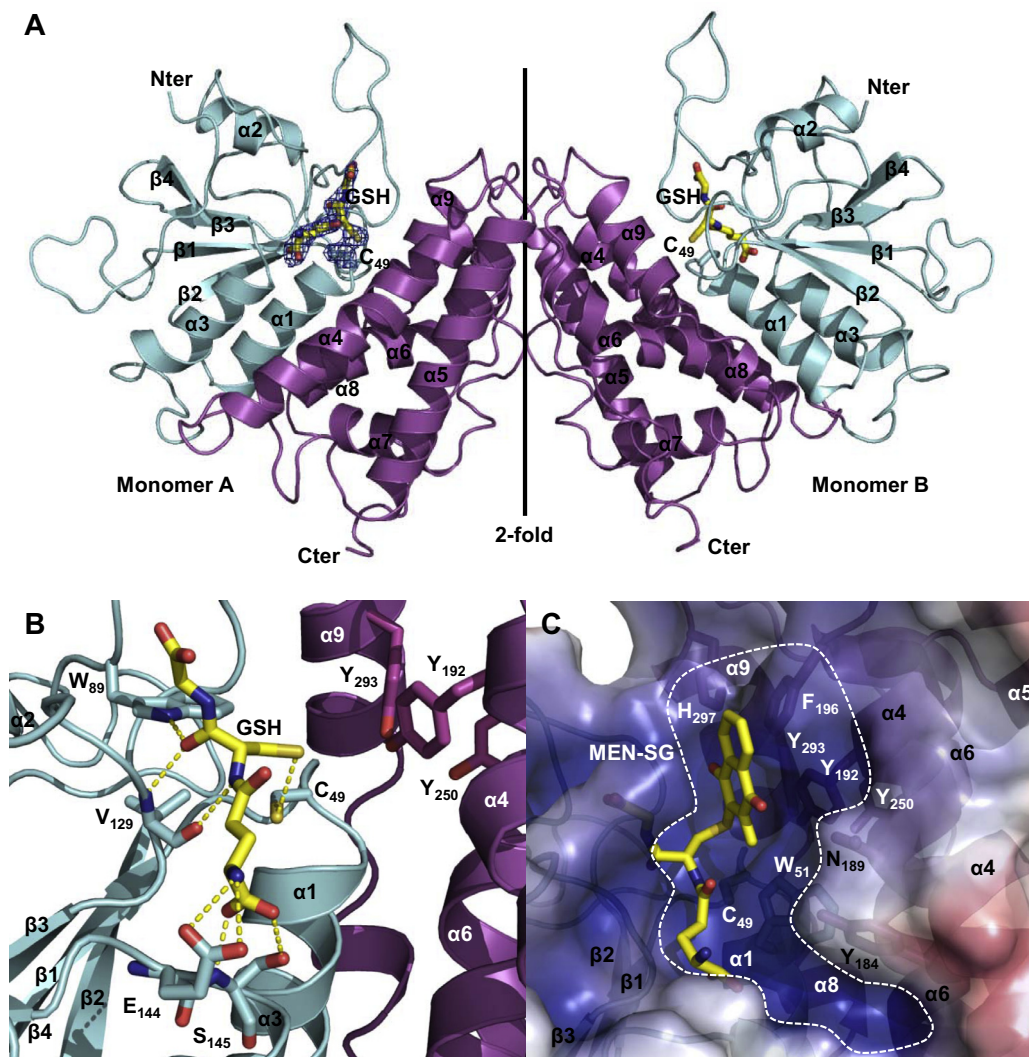


Fig. 3. 3D structure of Pt-GHR1 in complex with glutathione. (A) Cartoon representation of the overall structure of the dimeric Pt-GHR1. The N- and C-terminal domains are shown in cyan and magenta, respectively. Glutathione (GSH) and the catalytic cysteine are shown as sticks. The final $2F_o - F_c$ electron density map (1.0σ) is shown in light blue and covering only the GSH molecule and catalytic cysteine of only one monomer (left monomer) to avoid overwriting of the figure. The secondary structures are labeled. (B) Glutathione binding site of Pt-GHR1. The catalytic cysteine (Cys49) and the residues involved in polar non-covalent interactions between the protein and GSH are represented as sticks. The putative polar interactions are shown as dashed lines. (C) Structure of the putative H-site of Pt-GHR1. The electrostatic surface (blue, positive charge; red, negative charge) of Pt-GHR1 in the region of GSH (shown as sticks) is superimposed with glutathionyl-menadione (sticks) bound in the active site of Ec-YqjG (PDB code: 4GOK) [18]. A cleft visible in the vicinity of the G-site could accommodate the non-glutathione moiety of the substrate. Residues delimiting this pocket are shown as sticks and labeled.

Five Xi GST (GSTX) structures were previously determined but none from plants: GHR1 from *P. chrysosporium* (Pc-GHR1, pdb entry code 3PPU), YqjG from *E. coli* (Ec-YqjG, 4G0I), PcpF from *S. chlorophenolicum* (Sc-PcpF, 4FQU), GSTX from *Corynebacterium glutamicum* (Cg-GSTX, 3M1G) and GSTX from *Gordonia bronchialis* (Gb-GSTX, 4PTS) (Fig. S1) [8,18,26,27]. All these GSTXs share the same general fold and dimer organization (Fig. S1). A GSTX monomer consists of an N-terminal thioredoxin-like motif ($\beta 1\alpha 1\beta 2\alpha 2\beta 3\beta 4\alpha 3$) and an α -helical C-terminal domain ($\alpha 4\alpha 5\alpha 6\alpha 7\alpha 8\alpha 9$) (Fig. 3A). α Superimpositions revealed that the main differences between GSTXs are located in the N- and C-terminal extensions and in the $\beta 2$ - $\alpha 2$ loop whose lengths can vary significantly from one structure to another (root mean square deviation ranging from 0.54 Å to 0.89 Å for a minimum of 208 superimposed C α) (Fig. S1). For instance, Pt-GHR1 has the shortest N-terminal extension and does not exhibit the small three-stranded β -sheet observed in this region in Ec-YqjG and Sc-PcpF. However, these differences do not affect the monomer–monomer contacts

that exclusively involve the C-terminal domains (Fig. S1) [8,18,26,27]. Due to this specific dimerization mode, the $\alpha 6$ - $\alpha 7$ loops of both monomers are in close vicinity. The C-terminal loop part, which is antiparallel to $\alpha 9$, interacts with the N-terminal part of $\alpha 5$ and with the $\alpha 6$ - $\alpha 7$ loop of the other monomer. The comparison of the GSTX dimer interfaces reveals that the number of polar contacts ranges from 12 to 16. The hydrogen bonds between the carboxamide group of Q200 (Pt-GHR1 numbering) and the main chain atoms of I306 are the only tight interactions that are present in all known GSTX structures (Fig. S2). This relatively low conservation could be explained by the fact that the dimer interface mainly involves loops, *i.e.* regions in which sequence modifications due to evolution are more frequent.

In Pt-GHR1, the glutathione molecule forms hydrogen bonds with V129 and S145 main chain atoms and with W89, E144 and S145 side chains (Fig. 3B). Of these residues, only W89 is specific to GHRs. Interestingly, the E144–S145 pair, well conserved in most GST classes, is replaced by D150–Y151 and D139–F140 pairs in

Cg-GSTX and Gb-GSTX, respectively. In both cases, aromatic side chains occupy the G-site which would preclude glutathione binding raising the question of the GHR activity of these GSTXs.

Residues delimiting the H-site have been identified previously from the crystal structure of Ec-YqjG in complex with glutathionyl-menadione [18]. The corresponding residues, W51 from the CPWA active site motif, Y184, N189, Y192, F196 in $\alpha 4$ and H297 in $\alpha 9$ are conserved in Pt-GHR1 and maintain a similar H-site architecture (Fig. 3C). The catalytic tyrosine triad, which provides the proton needed for reductive deglutathionylation [18] is also conserved with Tyr found at positions 192, 250 and 293 in helices $\alpha 4$, $\alpha 6$ and $\alpha 9$, respectively. Interestingly, the H-site residues of GSTOs and GSTLs are more variable from one organism to another. This could be due to the ability of these proteins to deglutathionylate a broader substrate spectrum compared to GHRs that are specialized in quinone-SG reduction.

3.4. Enzymatic properties of Pt-GHR1

The enzymatic activities of Pt-GHR1 and mutated variants were assayed for various substrates. No significant peroxidase, esterase or glutathionylation activities were detected whereas Pt-GHR1 exhibited deglutathionylation activities with hydroxyethyl disulfide (HED) and dehydroascorbate (DHA) (Table 2). Although Pt-GHR1 exhibited comparable affinities toward DHA and HED (770 and 400 μM respectively), the catalytic efficiency for HED is about 30 fold higher essentially due to higher turnover (29.40 s^{-1} for HED vs 1.85 s^{-1} for DHA). Nevertheless, the recorded catalytic efficiencies and turnover numbers are of the same order of magnitude as those obtained for fungal GSTOs [21], bacterial (Ec-YqjG and Sc-PcpF) [6] and fungal (Pc-GHR1) [8] GHRs and plant GSTLs [16].

Then, we tested glutathionyl-quinone derivatives (glutathionylated menadione (MEN-SG), 1,4-benzoquinone (BQ-SG) and one chlorinated derivative, 2-chloro-1,4-benzoquinone (ClBQ-SG)), glutathionyl-ketone derivatives (glutathionylated phenylacetophenone (PAP-SG) or tetralone (TETRA-SG)) usually recognized by GSTLs or GSTOs [16,21] and glutathionyl-flavonol derivative (glutathionylated quercetin (Q-SG)), as a representative GSTL substrate [28]. Pt-GHR1 was able to deglutathionylate all quinone derivatives and Q-SG (Tables 2 and 3). For Q-SG, although Pt-GHR1 exhibits a high apparent affinity (K_m of 2.68 μM), the velocity (0.013 s^{-1}) and thus the catalytic efficiency are weak, as found with Pt-GSTLs [16] and Grxs (data not shown). These results suggest that Q-SG reduction may represent some sort of diaphorase activity linked to the presence of an exposed reactive cysteine. Concerning quinone derivatives, catalytic efficiencies range from $1.74 \times 10^4 \text{ M}^{-1} \text{ s}^{-1}$ for MEN-SG to $1.10 \times 10^5 \text{ M}^{-1} \text{ s}^{-1}$ for ClBQ-SG. Although Pt-GHR1

displays activity towards HED, DHA and Q-SG, the observation that GHRs are the only plant Cys-GSTs catalyzing the deglutathionylation of GSH-conjugated quinones and with the best catalytic parameters suggests that they might represent physiological substrates. All enzymatic activities are dependent on the presence of the catalytic cysteine since Pt-GHR1 C49S displayed less than 1% activity compared to Pt-GHR1 and the activity of Pt-GHR1 C49A was totally abolished (Table 2).

3.5. Activity with glutathionylated quinones: oxidized vs reduced forms

Previous studies showed that several bacterial and fungal GHRs are able to deglutathionylate glutathionyl-hydroquinone forms, but not a glutathionyl-benzoquinone as menadione-SG [9], unlike Pc-GHR1 [8]. Thus, menadione-SG was used to investigate the properties of Pt-GHR1 in comparison to Pc-GHR1 and Ec-YqjG. In vitro synthesized menadione-SG led to the formation of two different products that could be separated by HPLC, a minor peak with a molecular mass of 479Da and a major peak with a molecular mass of 477Da, consistent with menadiol-SG and menadione-SG respectively. These two forms can also be differentiated from their UV/visible absorbance spectra since menadione-SG (Fig. 4A, curve b) exhibits a characteristic absorption band centered at 430 nm which is absent in menadione (Fig. 4A, curve a), menadiol (Fig. 4A, curve c) and menadiol-SG spectra (Fig. 4A, curve d). We have also verified that NaBH_4 , but not GSH, was able to reduce

Table 3
Kinetic parameters of GHRs towards menadione-SG and menadiol-SG.

	Menadione-SG	Menadiol-SG
K_m (mM)		
Pt-GHR1	0.27 ± 0.00	0.003 ± 0.001
Pc-GHR1	2.00 ± 0.62	0.007 ± 0.001
Ec-YqjG	1.20 ± 0.30	0.025 ± 0.003
k_{cat} (s^{-1})		
Pt-GHR1	4.75 ± 0.30	9.42 ± 0.57
Pc-GHR1	19.60 ± 2.30	27.90 ± 1.07
Ec-YqjG	23.80 ± 1.90	40.98 ± 0.90
k_{cat}/K_m ($\text{M}^{-1} \text{s}^{-1}$)		
Pt-GHR1	$17.37 \times 10^3 \pm 1.10 \times 10^3$	$3215.10 \times 10^3 \pm 192.47 \times 10^3$
Pc-GHR1	$9.80 \times 10^3 \pm 0.32 \times 10^3$	$4019.25 \times 10^3 \pm 154.05 \times 10^3$
Ec-YqjG	$19.20 \times 10^3 \pm 0.33 \times 10^3$	$1659.03 \times 10^3 \pm 36.53 \times 10^3$

Menadiol-SG was obtained by reduction of menadione-SG using NaBH_4 . Kinetics parameters were determined from initial velocity using varying substrate concentrations at saturating GSH concentration by fitting the results to the Michaelis-Menten equation using GraphPad Prism 5 software. Data are represented as mean ± S.D. (n = 3). ND: not detected.

Table 2
Kinetic parameters of Pt-GHR1.

	HED	DHA	Q-SG	BQ-SG	ClBQ-SG
K_m (μM)					
Pt-GHR1	400.00 ± 40.00	770.00 ± 70.00	2.68 ± 0.26	92.59 ± 16.94	71.96 ± 8.60
Pt-GHR1 C49S	80.00 ± 10.00	nd	nd	nd	nd
Pt-GHR1 C49A	nd	nd	nd	nd	nd
k_{cat} (s^{-1})					
Pt-GHR1	29.40 ± 0.87	1.85 ± 0.07	0.013 ± 0.0004	1.62 ± 0.15	7.96 ± 0.33
Pt-GHR1 C49S	0.22 ± 0.01	nd	nd	nd	nd
Pt-GHR1 C49A	nd	nd	nd	nd	nd
k_{cat}/K_m ($\text{M}^{-1} \text{s}^{-1}$)					
Pt-GHR1	$73.62 \times 10^3 \pm 2.17 \times 10^3$	$2.39 \times 10^3 \pm 0.10 \times 10^3$	$4.95 \times 10^3 \pm 0.16 \times 10^3$	$17.50 \times 10^3 \pm 1.58 \times 10^3$	$110.60 \times 10^3 \pm 4.52 \times 10^3$
Pt-GHR1 C49S	$2.74 \times 10^3 \pm 0.07 \times 10^3$	nd	nd	nd	nd
Pt-GHR1 C49A	nd	nd	nd	nd	nd

Catalytic parameters were determined using varying substrate concentrations at saturating GSH concentration by fitting the results to the Michaelis-Menten equation using GraphPad Prism 5 software. Data are represented as mean ± S.D. (n = 3). ND: not detected. HED: hydroxyethyl disulfide, DHA: dehydroascorbate, Q-SG: glutathionylated quercetin, BQ-SG: glutathionylated 1,4-benzoquinone, ClBQ-SG: glutathionylated 2-chloro-1,4-benzoquinone.

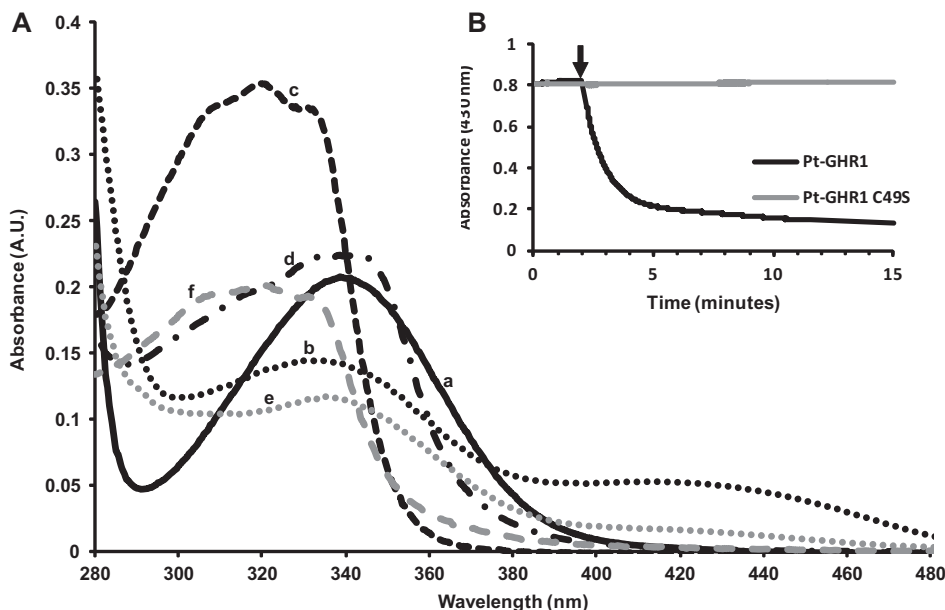


Fig. 4. Enzymatic reduction of menadione-SG and menadiol-SG by Pt-GHR1. (A) UV/visible spectra (280–480 nm) of menadione-SG and menadiol-SG incubated with or without Pt-GHR1. Spectra were recorded using 100 μM of menadione (a), menadione-SG (b), menadiol (c) and menadiol-SG (d). Menadiol and menadiol-SG have been obtained after a 15 s incubation with 1 mM NaBH_4 . Deglutathionylation of menadione-SG (100 μM) into menadione (e) or menadiol-SG (100 μM) into menadiol (f) was performed using 1.5 μM recombinant Pt-GHR1 in the presence of 1 mM GSH. The spectra have been recorded once substrate transformation is complete (around 1 min for menadiol-SG and 15 min for menadione-SG). (B) Deglutathionylation of menadione-SG by Pt-GHR1 and Pt-GHR1 C49S. After 2 min incubation of 300 μM menadione-SG with 2 mM glutathione, the activity was recorded by adding recombinant enzymes (10 μM) and following the decrease of absorbance at 430 nm.

menadione-SG into menadiol-SG in solution. When menadione-SG pre-incubated or not with NaBH_4 was further incubated with GSH and Pt-GHR1 (Fig. 4A, curves e, f), Ec-YqjG (Fig. S3) or Pc-GHR1 (Fig. S4), the changes in the UV/visible spectra indicated that all enzymes can deglutathionylate both menadione-SG into menadione and menadiol-SG into menadiol. The analysis of the same reaction mixtures by liquid chromatography coupled to mass spectrometry showed a single product with a molecular mass of 172Da and a UV/visible spectrum similar to menadione (data not shown). The fact that only menadione was detected for NaBH_4 -treated samples can be explained by the rapid oxidation of menadiol into menadione. In single turnover experiments using reduced proteins in the absence of GSH, subsequent mass spectrometry analyses indicated that the proteins are glutathionylated. Hence, as reported for some GHRs, GSTOs or GSTLs, a glutathionylated enzyme likely constitutes a catalytic intermediate [8,16,21]. Complementary kinetic experiments were carried out specifically on menadione-SG by monitoring the variation of absorbance at 430 nm with saturating amounts of GSH in the absence of NaBH_4 . A decrease in the absorbance at 430 nm was observed only with Pt-GHR1, Pc-GHR1 or Ec-YqjG but not with cysteinic variants (Pt-GHR1 C49S, Pc-GHR1 C86S and Ec-YqjG C63S) (Figs. 4B, S3 and S4). Enzymatic parameters were determined by following the decrease of menadione-SG or menadiol-SG concentration by HPLC. Overall, the three GHRs have comparable turnover numbers (k_{cat}) for the two substrates. However, apparent K_m values are responsible for large variations in catalytic efficiencies (Table 3). For example, Pt-GHR1 exhibits apparent K_m values of 273 μM and 3 μM respectively for menadione-SG and menadiol-SG resulting in a 185 fold higher catalytic efficiency towards menadiol-SG ($3.22 \times 10^6 \text{ M}^{-1} \text{ s}^{-1}$) as compared to menadione-SG ($1.7 \times 10^4 \text{ M}^{-1} \text{ s}^{-1}$). Hence, in contrast to *S. cerevisiae* ECM4 [9], all tested GHRs are able to catalyze the deglutathionylation of both menadione-SG and menadiol-SG, although with a clear preference for the latter. However, the question of the physiological substrates of plant GHRs is still open since the major quinone forms found in plastids/chloroplasts, plastoquinones, phylloquinones or

α -tocopherol, are present in membranes and do not have electrophilic sites susceptible to react spontaneously with GSH via Michael addition.

Acknowledgments

This work was supported by a grant from ANR as part of the “Investissements d’Avenir” program (ANR-11-LABX-0002-01, Lab of Excellence ARBRE). We thank Karin Krupinska (Kiel University, Germany) and René Lorbiecke (Hamburg University, Germany) for the gift of the PENDING:dsRED plasmid. We also thank Patrick Weber for performing robot-driven crystallization trials. We acknowledge SOLEIL for providing synchrotron radiation facilities, and we thank the staff of PROXIMA-1 beamline for assistance.

Appendix A. Supplementary data

Supplementary data associated with this article can be found, in the online version, at <http://dx.doi.org/10.1016/j.febslet.2014.11.021>.

References

- Jacquot, J.P., Dietz, K.J., Rouhier, N., Meux, E., Lallement, P.A., Selles, B. and Hecker, A. (2013) Redox regulation in plants: glutathione and “redoxin” related families in: Oxidative Stress and Redox Regulation (Daniel, E.E., Ed.), pp. 213–231, Springer, Netherlands.
- Liu, Y.J., Han, X.M., Ren, L.L., Yang, H.L. and Zeng, Q.Y. (2013) Functional divergence of the glutathione S-transferase supergene family in *Physcomitrella patens* reveals complex patterns of large gene family evolution in land plants. *Plant Physiol.* 161, 773–786.
- Rezaei, M.K., Shobbar, Z.S., Shahbazi, M., Abedini, R. and Zare, S. (2013) Glutathione S-transferase (GST) family in barley: identification of members, enzyme activity, and gene expression pattern. *J. Plant Physiol.* 170, 1277–1284.
- Lallement, P.A., Brouwer, B., Keech, O., Hecker, A. and Rouhier, N. (2014) The still mysterious roles of cysteine-containing glutathione transferases in plants. *Front. Pharmacol.* 5, 192.
- Morel, M., Ngadin, A.A., Droux, M., Jacquot, J.P. and Gelhaye, E. (2009) The fungal glutathione S-transferase system. Evidence of new classes in the wood-degrading basidiomycete *Phanerochaete chrysosporium*. *Cell Mol. Life Sci.* 66, 3711–3725.

- [6] Xun, L., Belchik, S.M., Xun, R., Huang, Y., Zhou, H., Sanchez, E., Kang, C. and Board, P.G. (2010) S-glutathionyl-(chloro)hydroquinone reductases: a novel class of glutathione transferases. *Biochem. J.* 428, 419–427.
- [7] Belchik, S.M. and Xun, L. (2011) S-glutathionyl-(chloro)hydroquinone reductases: a new class of glutathione transferases functioning as oxidoreductases. *Drug Metab. Rev.* 43, 307–316.
- [8] Meux, E., Prosper, P., Ngadin, A., Didierjean, C., Morel, M., Dumarcay, S., Lamant, T., Jacquot, J.P., Favier, F. and Gelhaye, E. (2011) Glutathione transferases of *Phanerochaete chrysosporium*: S-glutathionyl-p-hydroquinone reductase belongs to a new structural class. *J. Biol. Chem.* 286, 9162–9173.
- [9] Lam, L.K., Zhang, Z., Board, P.G. and Xun, L. (2012) Reduction of benzoquinones to hydroquinones via spontaneous reaction with glutathione and enzymatic reaction by S-glutathionyl-hydroquinone reductases. *Biochemistry* 51, 5014–5021.
- [10] Huang, Y., Xun, R., Chen, G. and Xun, L. (2008) Maintenance role of a glutathionyl-hydroquinone lyase (PcpF) in pentachlorophenol degradation by *Sphingobium chlorophenolicum* ATCC 39723. *J. Bacteriol.* 190, 7595–7600.
- [11] Barreto, L., Garcera, A., Jansson, K., Sunnerhagen, P. and Herrero, E. (2006) A peroxisomal glutathione transferase of *Saccharomyces cerevisiae* is functionally related to sulfur amino acid metabolism. *Eukaryot. Cell* 5, 1748–1759.
- [12] Dixon, D.P., Davis, B.G. and Edwards, R. (2002) Functional divergence in the glutathione transferase superfamily in plants. Identification of two classes with putative functions in redox homeostasis in *Arabidopsis thaliana*. *J. Biol. Chem.* 277, 30859–30869.
- [13] Board, P.G., Coggan, M., Chelvanayagam, G., Easteal, S., Jermiin, L.S., Schulte, G.K., Danley, D.E., Hoth, L.R., Griffon, M.C., Kamath, A.V., Rosner, M.H., Chrunk, B.A., Perregaux, D.E., Gabel, C.A., Geoghegan, K.F. and Pandit, J. (2000) Identification, characterization, and crystal structure of the Omega class glutathione transferases. *J. Biol. Chem.* 275, 24798–24806.
- [14] Rossjohn, J., Polekhina, G., Feil, S.C., Allocati, N., Masulli, M., Di Illio, C. and Parker, M.W. (1998) A mixed disulfide bond in bacterial glutathione transferase: functional and evolutionary implications. *Structure* 6, 721–734.
- [15] Garcera, A., Barreto, L., Piedrafita, L., Tamarit, J. and Herrero, E. (2006) *Saccharomyces cerevisiae* cells have three Omega class glutathione S-transferases acting as 1-Cys thiol transferases. *Biochem. J.* 398, 187–196.
- [16] Lallement, P.A., Meux, E., Gualberto, J.M., Prosper, P., Didierjean, C., Saul, F., Haouz, A., Rouhier, N. and Hecker, A. (2014) Structural and enzymatic insights into Lambda glutathione transferases from *Populus trichocarpa*, monomeric enzymes constituting an early divergent class specific to terrestrial plants. *Biochem. J.* 462, 39–52.
- [17] Couturier, J., Jacquot, J.P. and Rouhier, N. (2013) Toward a refined classification of class I dithiol glutaredoxins from poplar: biochemical basis for the definition of two subclasses. *Front. Plant Sci.* 4, 518.
- [18] Green, A.R., Hayes, R.P., Xun, L. and Kang, C. (2012) Structural understanding of the glutathione-dependent reduction mechanism of glutathionyl-hydroquinone reductases. *J. Biol. Chem.* 287, 35838–35848.
- [19] Menand, B., Marechal-Drouard, L., Sakamoto, W., Dietrich, A. and Wintz, H. (1998) A single gene of chloroplast origin codes for mitochondrial and chloroplastic methionyl-tRNA synthetase in *Arabidopsis thaliana*. *Proc. Natl. Acad. Sci. U.S.A.* 95, 11014–11019.
- [20] Melonek, J., Matros, A., Trosch, M., Mock, H.P. and Krupinska, K. (2012) The core of chloroplast nucleoids contains architectural SWIB domain proteins. *Plant Cell* 24, 3060–3073.
- [21] Meux, E., Morel, M., Lamant, T., Gerardin, P., Jacquot, J.P., Dumarcay, S. and Gelhaye, E. (2013) New substrates and activity of *Phanerochaete chrysosporium* Omega glutathione transferases. *Biochimie* 95, 336–346.
- [22] Nickerson, W.J., Falcone, G. and Strauss, G. (1963) Studies on quinone-thioethers. I. Mechanism of formation and properties of thiodione. *Biochemistry* 2, 537–543.
- [23] Vince, R., Daluge, S. and Wadd, W.B. (1971) Studies on the inhibition of glyoxalase I by S-substituted glutathiones. *J. Med. Chem.* 14, 402–404.
- [24] van Ommen, B., Ploemen, J.H., Bogaards, J.J., Monks, T.J., Gau, S.S. and van Bladeren, P.J. (1991) Irreversible inhibition of rat glutathione S-transferase 1–1 by quinones and their glutathione conjugates. Structure-activity relationship and mechanism. *Biochem. J.* 276, 661–666.
- [25] Terasawa, K. and Sato, N. (2005) Visualization of plastid nucleoids *in situ* using the PEND-GFP fusion protein. *Plant Cell Physiol.* 46, 649–660.
- [26] Cuff, M. E., Marshall, N., Cobb, G. & Joachimiak, A. (2010) The structure of a putative glutathione S-transferase from *Corynebacterium glutamicum*, *Midwest Center for Structural Genomics Protein Structure Initiative*.
- [27] Kim, J., Toro, R., Bhosle, R., Al Obaidi, N. F., Morisco, L. L., Wasserman, S. R., Sojitra, S., Attonito, J. D., Scott Glenn, A., Chowdhury, S., Evans, B., Hillerich, B., Love, J., Seidel, R. D., Imker, H. J., Gerlt, J. A. & Almo, S. C. (2014) Crystal structure of a glutathione transferase from *Gordonia bronchialis* DSM 43247, target EFI-507405, *Enzyme Function Initiative*.
- [28] Dixon, D.P. and Edwards, R. (2010) Roles for stress-inducible lambda glutathione transferases in flavonoid metabolism in plants as identified by ligand fishing. *J. Biol. Chem.* 285, 36322–36329.